Testing the independence of partial thermoremanent magnetizations of single-domain and multidomain grains: Implications for paleointensity determination

Yongjae Yu[1,2] and David J. Dunlop[3]

Received 7 April 2006; revised 26 July 2006; accepted 1 August 2006; published 21 October 2006.

[1] The Thellier method of paleointensity determination requires that partial thermoremanent magnetizations (pTRMs) be additive, mutually independent, and reciprocal in their thermal blocking and unblocking. We tested the independence law by thermally demagnetizing a sum of orthogonal pTRMs produced by replacing part of an original TRM(T_C, T_0, $\boldsymbol{H}$) by pTRM(T, T_0, $\boldsymbol{H}$), with $\boldsymbol{H}$ rotated 90° between the TRM and the pTRM (T_C, Curie temperature; T_0, room temperature). The composite remanence simulates thermal remagnetization in nature. For single-domain grains, thermal demagnetization resolved the orthogonal pTRMs cleanly. Two remagnetization temperatures were tried, $T = 400$°C and 550°C; the latter gave a better test because the two pTRMs were almost equal. Directions were recovered to within ~5° for three of the four pTRMs, trajectories on vector diagrams intersected at exactly 400°C or 550°C, and the Arai plots were linear and yielded the correct field intensity for both pTRMs. However, multidomain magnetite violated the independence law. A remagnetization temperature $T = 400$°C produced almost equal pTRMs, but in thermal cleaning, because of overlap of their unblocking spectra they no longer appeared orthogonal. Each was displaced 13–15° toward the direction of the other as judged by quasi-linear segments on a vector diagram. The angle between the fields that produced the pTRMs thus appeared to be ~60°, not 90°. Arai plots for both pTRMs were strongly curved and yielded no usable paleointensity estimate. Phenomenological modeling correctly predicted the main results of the independence experiments.

Citation: Yu, Y., and D. J. Dunlop (2006), Testing the independence of partial thermoremanent magnetizations of single-domain and multidomain grains: Implications for paleointensity determination, *J. Geophys. Res.*, *111*, B12S31, doi:10.1029/2006JB004434.

1. Introduction

[2] The intensity variation of the ancient geomagnetic field provides important information about the evolution of the geodynamo, regimes of convection in the outer core, and growth of the inner core. The most widely used method of determining paleomagnetic field intensity is the Thellier method [*Thellier and Thellier*, 1959] and its variants [e.g., *Coe*, 1967; *Aitken et al.*, 1988]. In the Thellier experiment, fractions of a sample's natural remanent magnetization (NRM) are erased in ascending temperature steps, while in companion heating-cooling steps each lost NRM fraction is replaced by a partial thermoremanent magnetization (pTRM). This approach allows the underlying assumption that the pTRMs are additive, reciprocal and independent to be tested repeatedly in the course of the experiment.

[3] The Thellier laws [*Thellier*, 1938] were formulated for single-domain (SD) grains.

[4] 1. The additivity law is that partial TRMs produced in nonoverlapping blocking temperature intervals (T_i, T_{i-1}) are additive,

$$\mathrm{pTRM}(T_1, T_0) + \mathrm{pTRM}(T_2, T_1) + \cdots\cdots \mathrm{pTRM}(T_i, T_{i-1}) = \mathrm{pTRM}(T_i, T_0).$$

Experiments on magnetite have shown that additivity holds for SD, pseudosingle-domain (PSD) and multidomain (MD) grains alike [*Ozima and Ozima*, 1965; *Dunlop and West*, 1969; *Levi*, 1979; *McClelland and Sugiura*, 1987; *Shcherbakov and Sycheva*, 1997]. However, in the case of MD grains, there are two types of pTRMs, thermally cooled (TC) and thermally heated (TH) [*Vinogradov and Markov*, 1989]. A TC pTRM (T_i, T_0) is produced by zero-field heating to the Curie point (T_C) and cooling to T_i, at which time the field is turned on and the sample is cooled to room temperature (T_0). To produce a TH pTRM (T_i, T_0), the sample is heated in zero field to T_i (not to T_C) and then cooled in a field to T_0. TC pTRM obeys the additivity law but TH pTRM has a smaller intensity and does not [*Shcherbakova et al.*, 2000].

[1]Geosciences Research Division, Scripps Institution of Oceanography, La Jolla, California, USA.
[2]Now at Department of Earth and Environmental Sciences, Korea University, Seoul, South Korea.
[3]Geophysics, Department of Physics, University of Toronto, Toronto, Ontario, Canada.

0148-0227/06/2006JB004434$09.00

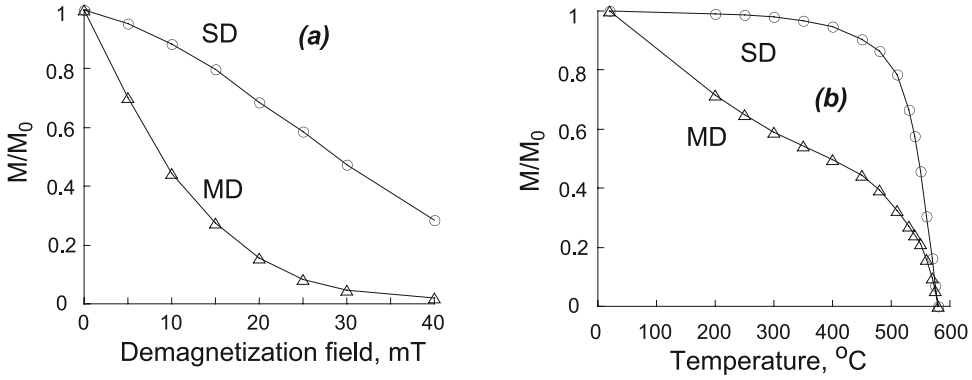

Figure 1. (a) Alternating field and (b) thermal demagnetization of total TRMs of single-domain (SD) and multidomain (MD) samples.

[5] 2. The reciprocity law is that pTRM (T_2, T_1) is demagnetized over the reciprocal interval (T_1, T_2). This law states the equivalence of the blocking temperature T_b at which pTRM is acquired during cooling and the unblocking temperature T_{ub} at which it demagnetizes during heating. In practice, part of a pTRM demagnetizes outside its blocking interval (T_2, T_1). The fraction with $T_{ub} < T_1$ represents a low-temperature tail of the T_{ub} spectrum, while the fraction with $T_{ub} > T_2$ is the high-temperature tail. Coarse-grained magnetites have large high-temperature tails [*Shashkanov and Metallova*, 1977; *Bol'shakov and Shcherbakov*, 1979; *Middleton and Schmidt*, 1982; *Dunlop*, 1983; *Worm et al.*, 1988; *Vinogradov and Markov*, 1989; *Halgedahl*, 1993; *McClelland et al.*, 1996; *Dunlop et al.*, 1997; *Shcherbakova et al.*, 1996, 2000; *Carlut and Kent*, 2002; *Carvallo et al.*, 2003; *Yu and Dunlop*, 2003; *Yu et al.*, 2004] as well as low-temperature tails [*Markov et al.*, 1983; *McClelland and Sugiura*, 1987; *Dunlop and Özdemir*, 2000; *Muxworthy*, 2000]. The T_{ub} spectrum of narrow-band (370–350°C) pTRMs broadens progressively with increasing magnetite grain size from near-SD to MD sizes [*Dunlop and Özdemir*, 2001].

[6] 3. The independence law is that pTRM (T_2, T_1) produced over the interval (T_2, T_1) is independent in direction and magnitude of pTRMs produced over intervals that do not overlap (T_2, T_1). The independence of nonoverlapping pTRMs is pivotal in both paleodirectional and paleointensity studies. Otherwise multivectorial NRMs cannot be resolved. Remagnetization in nature typically produces a multivectorial resultant. In addition, during pTRM steps in a Thellier experiment, the field is applied along the cylindrical axis of the sample, which is generally not the NRM direction. In our laboratory tests of independence, we replace part of a sample's TRM by an orthogonal pTRM, as in earlier pTRM studies [*Shcherbakov and Shcherbakova*, 2002; *Dunlop*, 2003] and in extensive testing of the independence of partial anhysteretic remanent magnetizations (pARMs) [*Yu et al.*, 2003]. Orthogonal pTRMs (or pARMs) have the advantage that the demagnetization of each can be tracked separately.

2. Sample Characterization

[7] We used six magnetite-bearing rocks with well-studied magnetic and paleomagnetic properties. For SD samples, we used three specimens of the Tudor Gabbro (Ontario, Canada), which yielded high-quality paleointensity data [*Yu and Dunlop*, 2001]. As MD samples, we used three specimens of the Cordova Gabbro [*Yu and Dunlop*, 2002] that had been rejected in paleointensity work because of their nonlinear Arai plots. During paleointensity work, the Tudor or Cordova samples used here showed negligible alteration in repeated heatings. All had pTRM checks within 5% of previous pTRMs in all temperature ranges. They also had low fabric anisotropy, an important consideration in testing independence by applying orthogonal fields. Plotted results are representative of the behavior of the entire sample set.

[8] Alternating field (AF) and thermal demagnetization curves of total TRM appear in Figure 1. TRM was produced by cooling from 600°C in a 50 μT field using a Shaw furnace. In AF demagnetization, an initial plateau is present for SD samples but absent for MD samples (Figure 1a). SD samples have a narrow TRM unblocking range (500–580°C) but MD samples unblock their TRM over a broad temperature range (Figure 1b).

3. Experimental Methods

[9] We tested independence by measuring thermal demagnetization of orthogonal pTRMs with nonoverlapping T_b intervals. Our procedure was as follows:

3.1. Independence Test

[10] First, we produced a total TRM by cooling from 600°C in a laboratory field $\boldsymbol{H}$ = 50 μT along the z direction. Then TRM_z was partially overprinted by $pTRM_x$ (T_i, T_0) produced by $\boldsymbol{H}$ = 50 μT along x. The vector resultant $\boldsymbol{M}$ was demagnetized in 50°C steps from 200–400°C, in 30°C steps to 510°C, in 10°C steps from 530–570°C, and at 575 and 580°C.

3.2. Paleointensity Simulation

[11] We produced a new bivectorial sum, TRM_z + $pTRM_x$, by the same procedure as in 1, replicating $\boldsymbol{M}$. Paleointensity determination was then simulated, following the *Coe* [1967] version of the Thellier method. After the first (zero-field) heating-cooling step to temperature T_j, the "NRM" remaining was measured. The second heating-cooling step to temperature T_j was in $\boldsymbol{H}$ = 50 μT along

the cylindrical z axis of the specimen. Subtraction of the first- and second-step remanences gave the pTRM acquired at T_j. Double heatings were carried out at the same steps as in 1, with pTRM checks at every second temperature. Temperatures in all heatings were reproducible within 1.3°C. The residual field in the furnace during "zero-field" heatings and coolings was <50 nT.

4. Modeling Demagnetization and Paleointensity Results

4.1. Phenomenological Modeling

[12] *Fabian* [2000, 2001] developed a phenomenological model of pTRM blocking and unblocking which closely parallels the classic *Preisach* [1935] model of hysteresis. The magnetic behavior of a sample is represented by a large number of independent cycles, each with a blocking temperature T_b and an unblocking temperature T_{ub}. The number of such cycles in a particular area of the T_{ub} versus T_b diagram is specified by the density function, $\lambda(T_b, T_{ub})$. Models based on Fabian's [*Biggin and Böhnel*, 2003; *Krása et al.*, 2003; *Leonhardt et al.*, 2004] or equivalent mathematical models [*Yu and Dunlop*, 2003; *Yu et al.*, 2004; *Yu and Tauxe*, 2005] can explain nonlinear Arai plots observed for coarse-grained magnetites [*Levi*, 1977; *Shcherbakov and Shcherbakova*, 2001; *Xu and Dunlop*, 2004; *Dunlop et al.*, 2005].

[13] In our phenomenological model, we set the cumulative sum of λ equal to 1. All remanences are then normalized to total TRM, represented vectorially as [0, 0, 1]. We deal with TH pTRMs which are the pTRMs produced in actual Thellier experiments. We define ten temperature steps T_j (T_1, T_2, …. T_9, T_C) such that each thermal demagnetization step in the ideal SD case destroys 10% of TRM and each incremental pTRM equals 10% of TRM. Subscripts and superscripts represent magnetization direction and temperature T_j, respectively. For example M_x^{400} is the x component of the bivectorial remanence $\boldsymbol{M}$ produced at T_j = 400°C.

[14] In a T_{ub} vs. T_b diagram, the density function $\lambda(T_b, T_{ub})$ for an ideal SD sample has equal values of 1/10 on each square down the diagonal since by the reciprocity law, $T_b = T_{ub}$. Our Tudor Gabbro samples contain magnetite grains that are nearly but not perfectly SD. A large part of each pTRM has $T_b = T_{ub}$ but we anticipate minor low- and high-T tails with $T_b \neq T_{ub}$. We therefore make each diagonal value of $\lambda(T_b, T_{ub})$ equal 162/1800 and each off-diagonal value equal 2/1800 (Figure 2a). The reciprocal part of each pTRM (grey square) is then 9 times as large as the tails.

[15] In the MD case, e.g., our Cordova Gabbro samples, the tails are expected to be much larger, possibly equal to the reciprocal part of the pTRM [*Dunlop and Özdemir*, 2001; *Yu and Dunlop*, 2003]. We thus set each diagonal grey square equal to 90/1800 and the sum of the nine off-diagonal squares also equal to 90/1800 (Figure 3a). The value of individual white squares decreases with distance from the diagonal. For example, pTRM(T_1, T_0) has values in ascending squares in the first column of 90, 18, 16, 14, 12, 10, 8, 6, 4, and 2. Values of TH-pTRM tails and TC-pTRM tails are half of these listed values. While TC-pTRM tails are demagnetized during zero-field steps, only TH-pTRM tails and reciprocal fractions are remagnetized during in-field steps. Real samples may have more complicated $\lambda(T_b, T_{ub})$, with possibly T-dependent tail/reciprocal pTRM ratios [*Yu and Dunlop*, 2003], but our model should be helpful in understanding the broad features of pTRM behavior.

[16] In simulating the Thellier experiment, we assume that $pTRM_x$ is produced between T_5 and T_0, making the intensity of $pTRM_x$ approximately one half of TRM_z. This is the case for two of our three experiments, described below. Our model TH $pTRM_x$ involves squares with T_b and T_{ub} both $\leq T_5$, while TRM_z magnetizes the entire five columns from T_5 to T_C on the T_b axis. Stepwise thermal demagnetization is modeled by erasing the remanence of successive rows parallel to the T_b axis at increasing T_{ub} levels. To simulate the Thellier experiment, we calculated pTRMs acquired between demagnetization steps by adding part columns with $T_{ub} \leq T_b$ at a particular T_b level.

4.2. SD Modeling Results

[17] In simulated thermal demagnetization of the composite NRM on a vector diagram (Figure 2b), the actual trajectories deviate by only 4.8° and 1.6° from ideal SD linear trajectories for M_x and M_z. Surviving TRM and overprinting pTRM thus demagnetize almost independently of each other. Deviation from the ideal lines is due to small pTRM tails (off-diagonal squares in Figure 2a).

[18] Conventional Arai plots [*Nagata et al.*, 1963] display multivectorial paleointensity data in a misleading way. For our model results, the Arai plot curves from T_0 to T_5, as if these data were unusable (Figure 2c). However, if we plot the scalar sum $M_x^{T5} + M_z^{T5}$ as NRM, the Arai plot is quasi-linear from T_0 to T_5 as well as from T_5 to T_C (Figure 2c). A better approach is to use multivectorial Arai plots [*Yu and Dunlop*, 2002], which track the thermal demagnetization of M_x and M_z separately (Figure 2d). The reciprocal fractions of M_x^{T5} and M_z^{T5} give slopes very close to −1, from $T_0 - T_5$ for M_x^{T5} and from $T_5 - T_C$ for M_z^{T5}. (Note that the NRM, $\boldsymbol{M}^{\mathbf{T5}}$, and all pTRMs in the Thellier experiment used the same field, $H = 50$ μT.) The contributions of the pTRM tails between T_0 and T_5 for M_z^{T5} and between T_5 and T_C for M_x^{T5} are minor.

4.3. MD Modeling Results

[19] In the MD case about 30% of M_z^{T5}, whose T_b are $\geq T_5$, demagnetizes below T_5 (Figure 3b). A smaller fraction (∼7%) of M_x^{T5}, which blocked between T_5 and T_0, unblocks above T_5. Demagnetization trajectories are more or less linear both above and below T_5 but deviate ∼40° and 7° from the ideal SD lines. As a result the angle between the TRM $\boldsymbol{M}_z^{\mathbf{T5}}$ and the pTRM overprint $\boldsymbol{M}_x^{\mathbf{T5}}$ appears to be only ∼45° instead of the actual 90°. Retrieving correct paleofield directions for either NRM component from the thermal demagnetization results is impossible.

[20] Thellier simulation results give convex-down curves in conventional, scalar sum and multivectorial Arai plots alike (Figures 3c and 3d). The symmetry of $\lambda(T_b, T_{ub})$ about the diagonal in the T_{ub} vs. T_b diagram (Figure 3a) results in similar trends for the two reciprocal pTRMs and for the two tail fractions in multivectorial Arai plots (Figure 3d): the trend of M_x ($T_0 - T_5$)

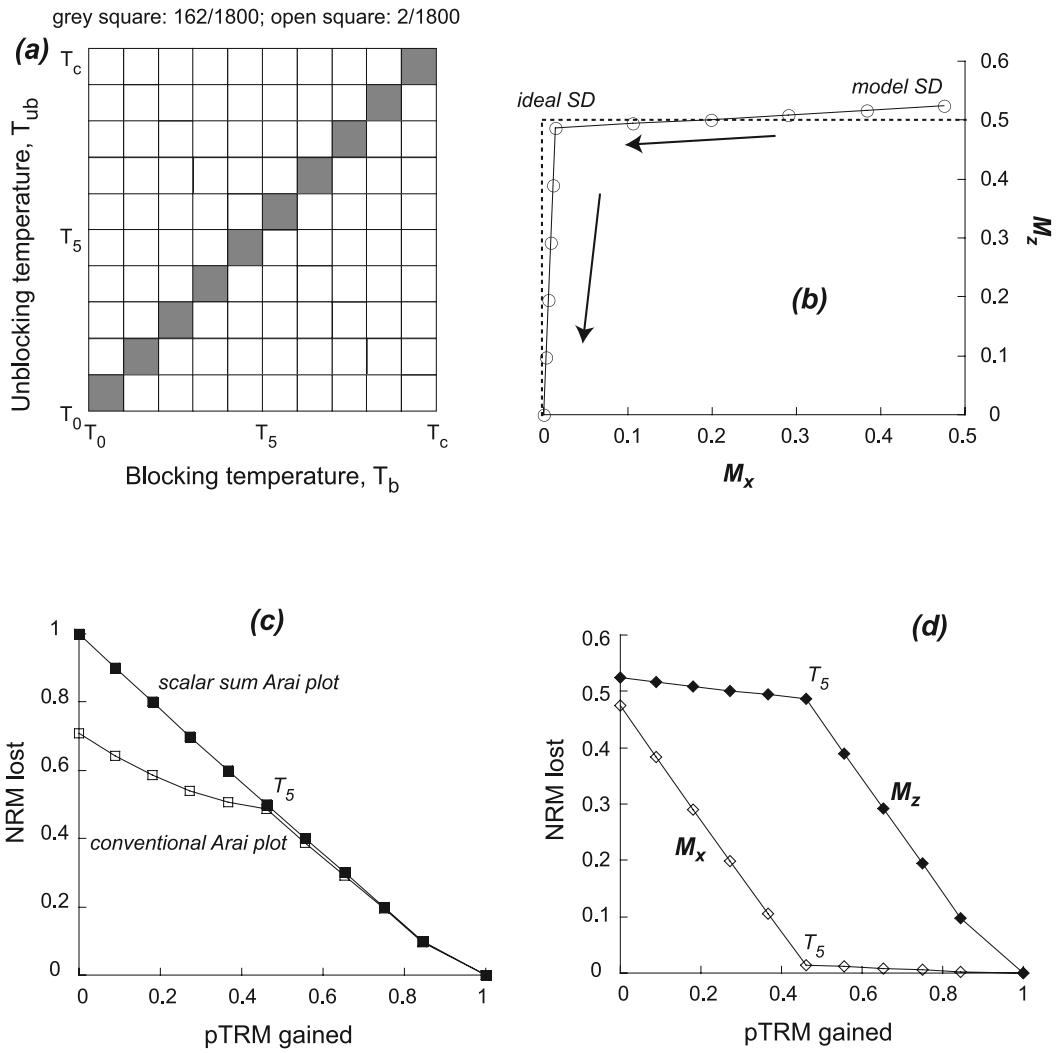

Figure 2. (a) SD model distribution $\lambda(T_b, T_{ub})$. The reciprocal part of pTRM is on the diagonal $T_{ub} = T_b$ (grey squares, 81 times the remanence of off-diagonal open squares). (b) Vector projection of model thermal demagnetization results. (c) and (d) Simulated conventional, scalar sum and multivectorial Arai plots.

resembles that of M_z ($T_5 - T_C$), and the trend of M_z ($T_0 - T_5$) resembles that of M_x ($T_5 - T_C$).

5. Experimental Results

5.1. SD Results

[21] For our SD samples, we first produced $\boldsymbol{M}$ with T_i = 400°C, chosen to match the MD experiment (next section). Thermal demagnetization curves of M_x^{400} (pTRM overprint), M_z^{400} (surviving TRM), the scalar sum $M_x^{400} + M_z^{400}$, and total TRM are shown in Figure 4a. As expected, M_x^{400} almost completely demagnetized by 400°C, satisfying reciprocity (Figure 4a). On the other hand, M_z^{400} unblocked almost entirely above 400°C, principally above 550°C (Figure 4a). Because M_x^{400} is so small compared to M_z^{400}, the low-T tail of M_z^{400} has a major effect on the demagnetization of the total remanence between 20 and 400°C. In vector projection, the short segment from 20 to 400°C deviates 17° from the x direction (Figure 4b). Conversely the high-T tail of M_x^{400} is too small to affect demagnetization between 400 and 580°C, and the long segment in Figure 4b over this T range is exactly parallel to z (calculated deviation of 0.2°). NRM vector projections thus follow the ideal SD line for any component whose magnitude is a substantial fraction of the total remanence, in this case M_z^{400}. In spite of the large low-T tail of M_z^{400}, the breakpoint between segments in Figure 4b is indistinguishable from 400°C (Figure 4b).

[22] Because of the preponderance of high T_{ub} we repeated the experiment with T_i = 550°C. The pTRM and TRM$_z$ intensities M_x^{550} and M_z^{550} are similar, and M_x unblocks almost entirely between 400 and 550°C, while M_z unblocks between 550 and 580°C (Figure 5a). In vector projection, NRM demagnetization trajectories are somewhat curved but have a sharp junction at the remagnetization temperature T_i = 550°C (Figure 5b). Best fit lines to the curved trajectories deviate 5.7° and 4.8° from the ideal lines for M_x and M_z, respectively (Figure 5b). Results of the Thellier experiment (Figures 5c and 5d) closely resemble the SD model results (Figures 2c and 2d). In particular, as predicted

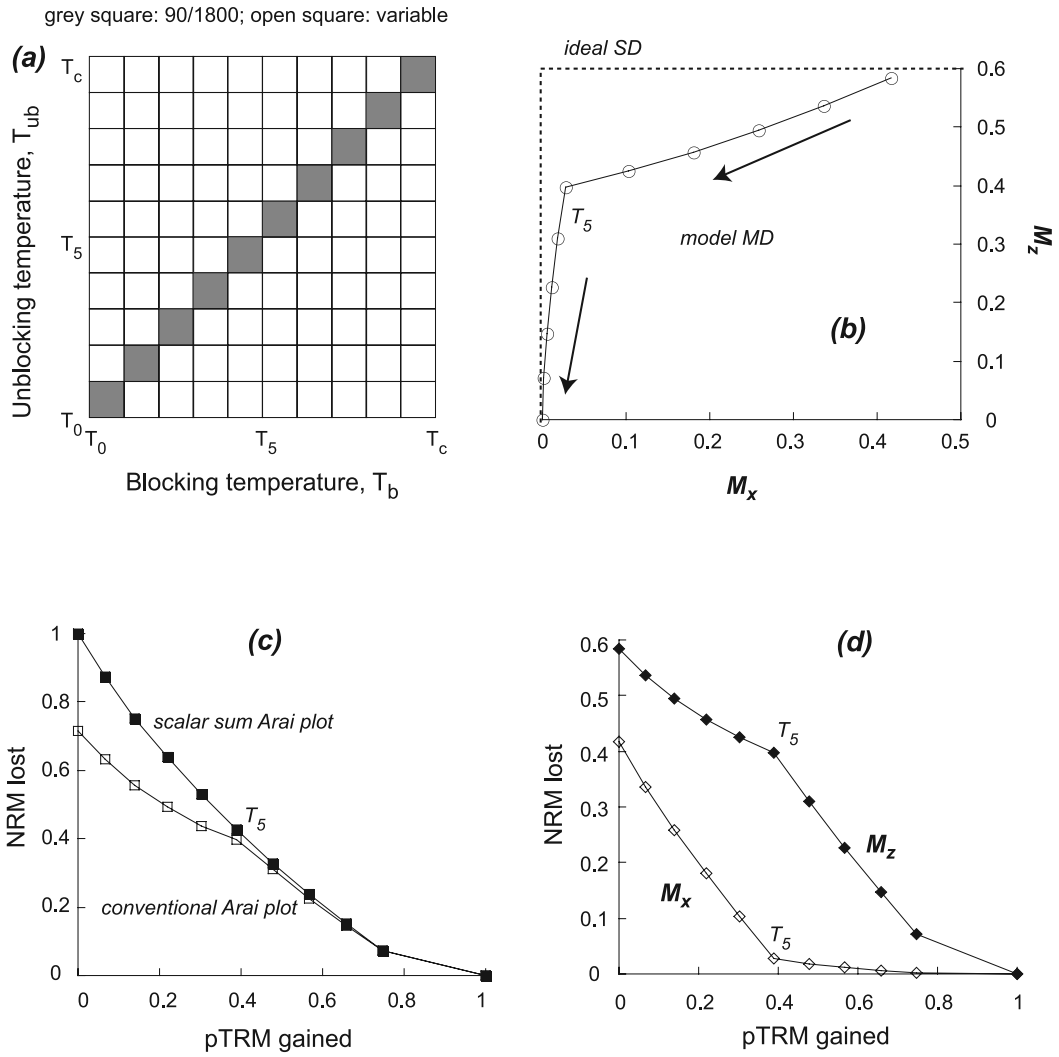

Figure 3. (a) MD model distribution $\lambda(T_b, T_{ub})$. Each diagonal grey square now has the same remanence as the sum of off-diagonal squares in the same column (reciprocal pTRM = pTRM tail). Values of open squares decrease away from the diagonal. (b) Vector projection of thermal demagnetization results. (c) and (d) Simulated conventional, scalar sum, and multivectorial Arai plots.

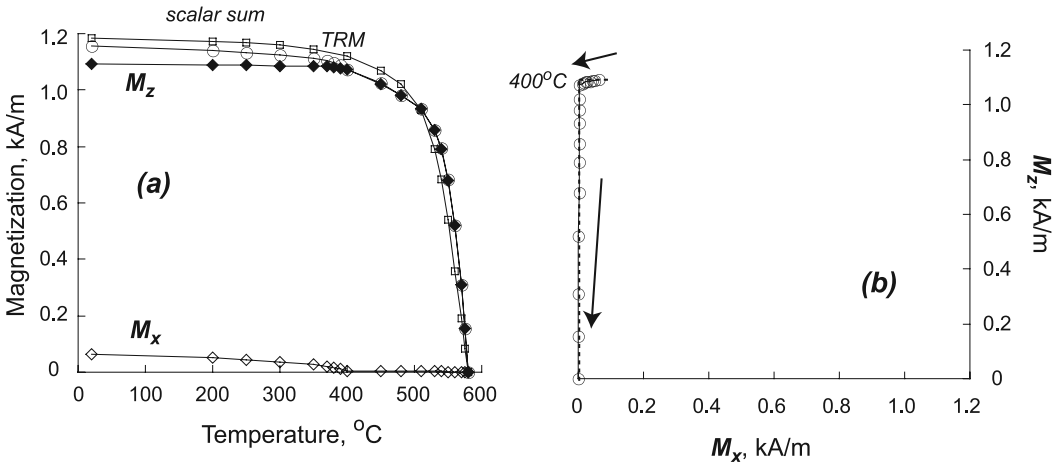

Figure 4. (a) Thermal demagnetization curves of $\boldsymbol{M}$ and its components M_z and M_x for an SD sample, compared with that of total TRM. $\boldsymbol{M}$ consists of TRM_z produced by cooling from 600°C in $\boldsymbol{H}$ = 50 μT along z overprinted by $pTRM_x$ (400°C, T_0, 50 μT) along x. (b) Demagnetization trajectory (vector plot), with ideal SD trajectories as dashed lines.

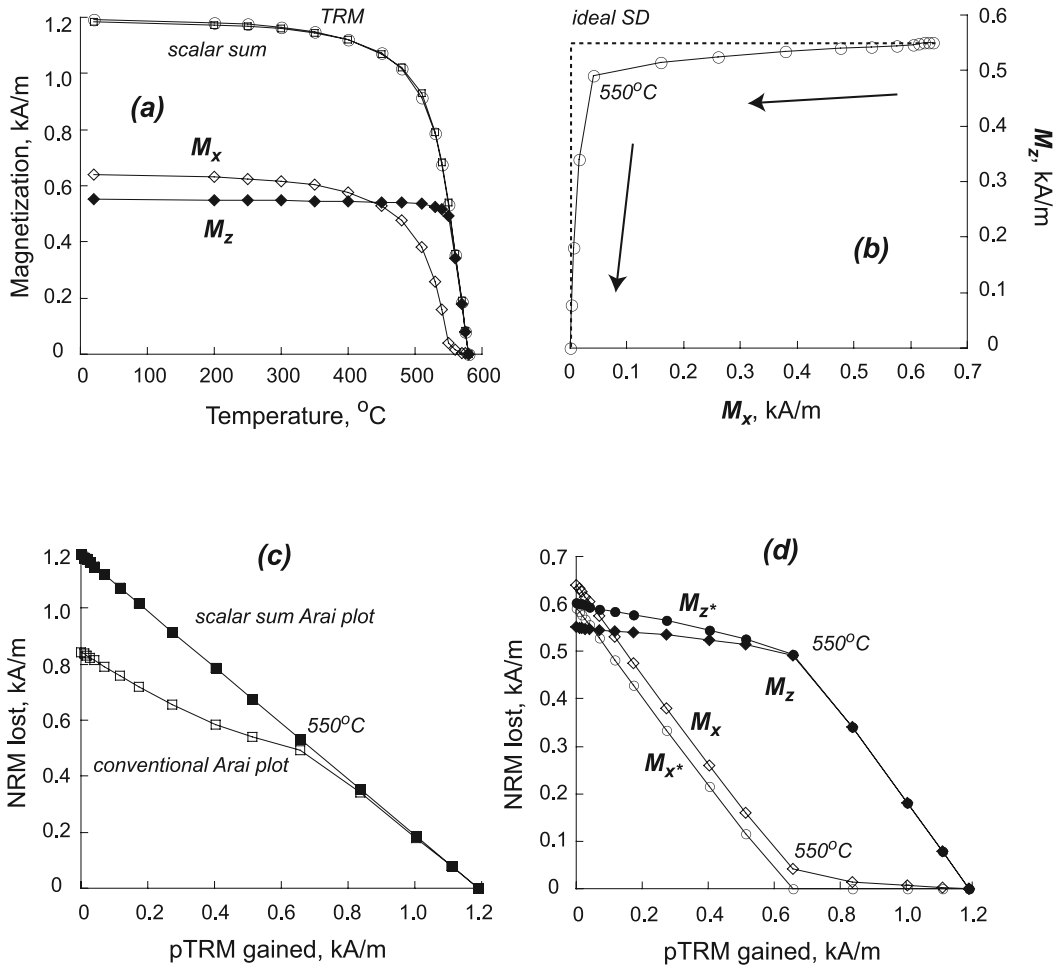

Figure 5. (a) Thermal demagnetization of $\boldsymbol{M}$ for the SD sample. In this case, $\boldsymbol{M}$ consists of TRM_z overprinted by $pTRM_x$ (550°C, T_0), giving approximately equal M_x and M_z. (b) Segments of the demagnetization trajectory, which are more curved than in Figure 4 and deviate by ~5° from x and z. (c) and (d) Arai plots of paleointensity data. The reciprocal fractions of M_x and M_z in Figure 5d yield correct field estimates despite some curvature of the segments. M_{x*} and M_{z*} were calculated using apparent directions from the data of Figure 5b rather than the known directions of M_x and M_z.

from the modeling, the multivectorial Arai plots yielded correct field intensities for both M_x^{550} and M_z^{550}, using the reciprocal fraction data (Figure 5d).

5.2. MD Results

[23] For the MD samples, we used T_i = 400°C which gives fairly similar magnitudes M_x^{400} and M_z^{400} (Figure 6a). M_x^{400} has a wide T_{ub} spectrum extending much above 400°C, while ~25% of M_z^{400} unblocks below 400°C. Unlike the model simulation, the experimental NRM vector projection is curved and has no obvious breakpoint (Figure 6b). To obtain an estimate of the junction temperature we followed standard paleomagnetic practice, fitting pairs of lines to the data and selecting the pair that yielded the highest k values for both M_x^{400} and M_z^{400}. This resulted in a junction temperature of 400°C, exactly reproducing T_i. The independence law is decisively violated: ~25% of M_z is demagnetized below 400°C, while the apparent pTRM direction is pulled 14.5° away from x toward z and the TRM direction is deflected 13.2° from z toward x (Figure 6b).

[24] We also explored other line fits to parts of the data set. For M_x, using the 20–350°C data gave I = 13.3°, MAD = 6.1° (maximum angular deviation [*Kirschvink*, 1980; *Tauxe*, 1998]), while the 20–400°C data gave I = 17.6°, MAD = 9.4°, compared to the true value I = 0°. For M_z, the 400–580°C data gave I = 81.3°, MAD = 2.0°, and the 480–580°C data gave I = 82.9°, MAD = 1.0°, compared to the true I = 90°. These are substantial errors of which paleomagnetists should be aware in attempting to use multivectorial NRMs from MD samples.

[25] Both conventional and scalar sum Arai plots are nonlinear and yield no acceptable field estimates for either component of $\boldsymbol{M}^{400}$ (Figure 6c). Even the Arai plots for the separated components are nonlinear. M_z^{400} is nearer to linearity than M_x (Figure 6d) but a best fitting line through the M_z data has a slope of −0.5 instead of the correct −1.

6. Discussion

[26] We tested pTRM independence by thermally demagnetizing orthogonal pTRMs produced by superimposing

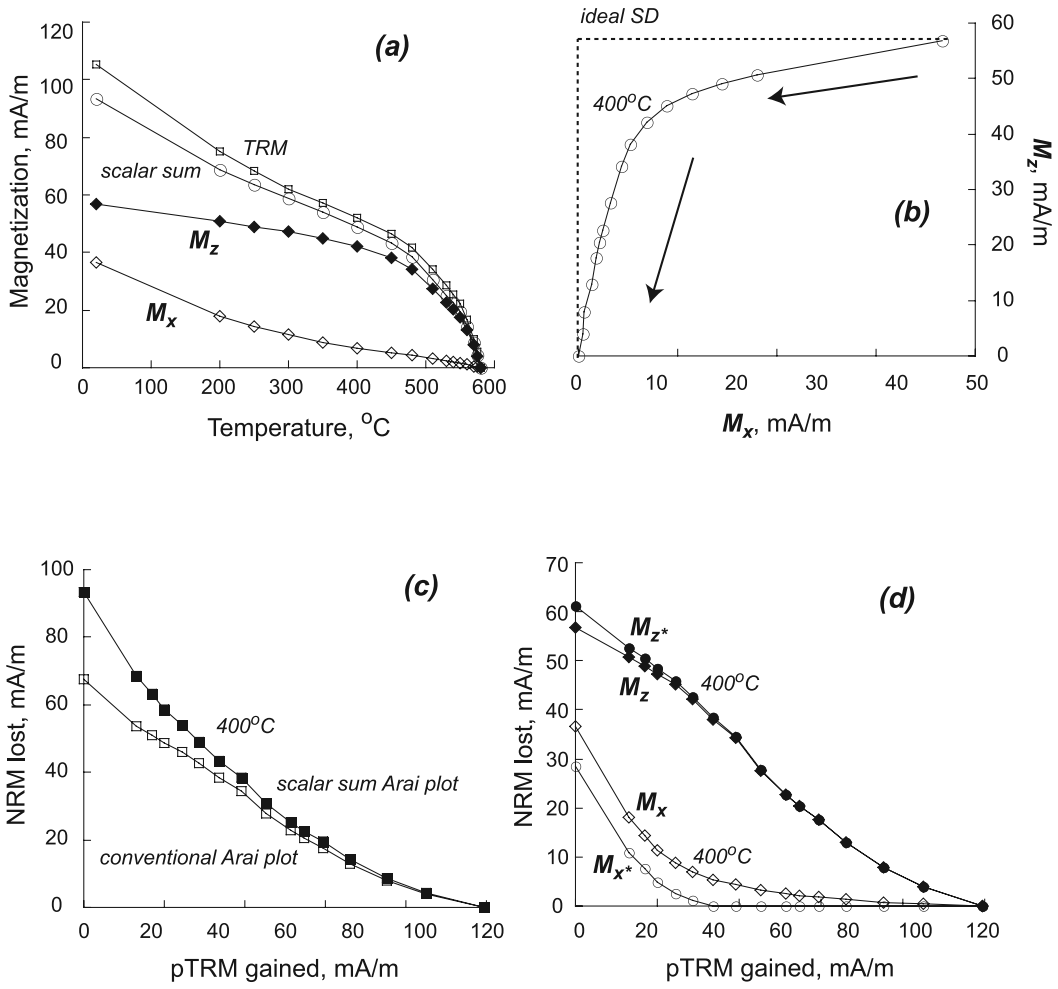

Figure 6. (a) Thermal demagnetization of $\boldsymbol{M}$ for an MD sample. $\boldsymbol{M}$ consists of TRM_z overprinted by $pTRM_x$ (400°C, T_0), giving $M_x \approx 2/3M_z$. (b) Demagnetization trajectory, which is strongly curved with no breakpoint, with deviations from x and z of ~15°. (c) and (d) Arai plots of paleointensity data. The multivectorial Arai curves in Figure 6d bear little resemblance to the model curves of Figure 3d. They are too curved to yield any meaningful field estimates.

$pTRM_x(T_i, T_0)$ on TRM_z. If the remaining TRM and the pTRM overprint are independent of each other, M_x should demagnetize completely in heating from T_0 to T_i and M_z should remain constant over the same range. The clearest way to display the results is in vector projections (Figures 2b, 3b, 4b, 5b, and 6b). Our SD samples came fairly close to ideal behavior, with deviations of $\leq 5°$ from straight-line trajectories along x and z for components of comparable magnitudes and sharp junctions at T_i between the trajectories (Figures 4b and 5b).

[27] In contrast, a superimposed $pTRM_x$ significantly affected the preexisting TRM_z for our MD samples. 25% of M_z^{400} was already demagnetized by 400°C and thermal demagnetization trajectories were quite curved on vector projections, with no easily recognizable junction temperature (Figure 6b). A standard paleomagnetic directional analysis would produce errors of 13–15° in estimates of the TRM and pTRM overprint directions.

[28] There are two insights relating to reciprocity and additivity to be gained from our data. First, even when there is significant violation of reciprocity, i.e., significant pTRM tails, it may be possible to obtain meaningful paleointensity values using only the reciprocal fraction of pTRM. For example, in Figure 5d M_x and M_z both give correct slopes of −1 in the reciprocal ranges of their Arai plots (20–550°C for M_x and 550–580°C for M_z), although both have pTRM tail fractions of 10% or more. Second, the scalar sum of M_x and M_z thermal demagnetization curves in Figures 4a, 5a, and 6a nearly matches the thermal demagnetization curves of SD or MD total TRM, explaining the widespread validity of the additivity law. Apparently a low-T tail of one remanence is compensated for by a high-T tail of the other remanence [*Dunlop and Özdemir*, 2001; *Dunlop*, 2003]. In the MD case, the scalar sum is ~10% less than total TRM at all T, reflecting the smaller tail of our TH $pTRM_x$ compared to a TC pTRM [e.g., *Shcherbakova et al.*, 2000].

[29] Phenomenological modeling was a useful indicator of experimental demagnetization and paleointensity results. For SD samples, test results were almost identical to the predictions of our model (Figures 2 and 5), suggesting that pTRM tails are small and symmetric about the diagonal, as modeled. A symmetric distribution of pTRM tails has been

demonstrated in measurements on narrow-band pTRMs [*Dunlop and Özdemir*, 2001] and from temperature-independent pTRM tail/total pTRM ratios [*Yu and Dunlop*, 2003]. A useful next step to test for symmetry directly would be to construct $\lambda(T_b, T_{ub})$ experimentally for a real SD sample using a set of measured pTRMs and thermal demagnetization data.

[30] For MD samples, there are some discrepancies between the modeling and experimental data (Figures 3 and 6). First, our model predicts quasi-linear trajectories with a sharp junction at T_5 in vector projections of thermal demagnetization data (Figure 3b) but experimentally the trajectories are strongly curved and have no breakpoint (Figure 6b). Second, in multivectorial Arai plots, the M_x and M_z reciprocal fraction segments are approximately parallel in model plots (Figure 3d) but not in experimental plots (Figure 6d). The model curves outline a quadrilateral but experimentally there are neither vertices (breakpoints) nor parallel sides. One reason is that these particular pTRMs have different magnitudes and their tails are not symmetric, violating the assumptions of our model. 25% of M_z demagnetizes below 400°C whereas <20% of M_x demagnetizes above 400°C; the contrast is heightened by the fact that M_x is <2/3 of M_z.

[31] The curved thermal demagnetization trajectories necessitated fitting pairs of straight lines in order to estimate the junction temperature T_i (Figure 6b). Standard paleomagnetic line fits maximizing the precision parameter k yielded lines intersecting very close to T_i. Our result is at odds with earlier observations where T_i was overestimated by 50°C [*Dunlop and Özdemir*, 1997, Figure 16.11; *Dunlop*, 2003]. This disagreement may result from different experimental conditions. We began with a total $\mathrm{TRM}_z(T_C, T_0)$, then heated to T_i and partially remagnetized the TRM with a perpendicular $\mathrm{pTRM}_x(T_i, T_0)$, giving a vector resultant $\boldsymbol{M}$. *Dunlop and Özdemir* [1997] cooled in a field from T_C and rotated the field by 90° at T_i, producing a vector resultant $\mathrm{pTRM}_z(T_C, T_i) + \mathrm{pTRM}_x(T_i, T_0)$ or $\boldsymbol{M}^*$. The two $\mathrm{pTRM}_x(T_i, T_0)$ are not equivalent. Theirs is a TC pTRM while ours is a TH pTRM, although superimposed on a magnetized rather than a demagnetized sample.

[32] Our model does not distinguish between $\boldsymbol{M}$ and $\boldsymbol{M}^*$, but experimentally it is well known that TH and TC pTRMs are not equivalent [e.g., *Shcherbakova et al.*, 2000]. Another factor is the initial state dependence of pTRM [e.g., *Yu and Tauxe*, 2006]. M_x remagnetizes a previously magnetized fraction of TRM with $T_b < T_i$ while M_x^* magnetizes an originally demagnetized $T_b < T_i$ fraction. If M_x^* is more resistant to thermal demagnetization than M_x, the breakpoint might migrate to a value higher than T_i. This question needs to be investigated experimentally and the results incorporated in a more sophisticated model that takes account of differences in the nature of pTRMs produced in different ways and from different initial states.

[33] It is important to construct separate Arai plots for each component in a multivectorial NRM. This separation can only be done rigorously if the direction of each vector is known. MD grains violate independence to such an extent that it is difficult or impossible to determine the component directions accurately (e.g., Figure 6b, where apparent directions of M_x and M_z, were 13–15° in error). In spite of this, the separate Arai plots of Figure 6d are similar whether constructed using known component directions (M_x, M_z) or raw data (M_{x*}, M_{z*}). In the SD case, directional estimates are more accurate, particularly for the higher-T_b pTRM (Figure 5b). A multivectorial Arai plot is then straightforward to construct and yields correct paleointensities for both primary and overprint magnetizations, whereas the conventional Arai plot gives no usable data for the overprint (Figures 5c and 5d).

7. Conclusions

[34] 1. Independence of pTRMs with nonoverlapping T_b ranges was verified for nearly SD magnetite grains. TRM demagnetized over a T_{ub} range that was almost exclusive of the T_{ub} range of an orthogonal overprinting pTRM. When the two remanences were of comparable magnitudes, their directions could be estimated to within ~5° from a vector projection of their demagnetization trajectories.

[35] 2. By plotting TRM and pTRM demagnetization data from a Thellier experiment separately (a multivectorial Arai plot), correct field intensities were determined for both remanences. This was accomplished by using only the fractions of TRM and pTRM that obeyed reciprocity, i.e., demagnetized over their respective T_b intervals.

[36] 3. For MD samples, an overprinting pTRM significantly affected the demagnetization of the original TRM and vice versa. Overlap of the two T_{ub} spectra was almost total and the nonreciprocal ($T_{ub} \neq T_b$) or "tail" fraction was 20–25% of either remanence. Demagnetization trajectories were strongly curved with no obvious junction temperature between components. Apparent directions of either remanence estimated from the trajectories were in error by ~15°. Thellier experiments gave continuously curving multivectorial Arai plots from which no meaningful field estimates could be calculated.

[37] 4. In spite of major violations of reciprocity and independence, MD grains obeyed the pTRM additivity law to within 10%, not only at room temperature but at every temperature from T_0 to T_C. In other words, the thermal demagnetization curves of pTRM and overprinted TRM when summed nearly matched the thermal demagnetization curve of total TRM.

[38] 5. The symmetry between low- and high-temperature tails in the T_{ub} spectra of the two remanences implied by conclusion 4 was embodied in the phenomenological model used to predict and interpret results: our density function $\lambda(T_b, T_{ub})$ was symmetrical about the diagonal of a T_{ub} vs. T_b diagram. This model, a derivative of *Fabian*'s [2000, 2001] models, was successful in predicting the SD experimental results but less successful for MD data. The match between predicted and observed results was improved by assuming values for off-diagonal elements of $\lambda(T_b, T_{ub})$ that decreased with distance from the diagonal. MD thermal data for a real sample could be inverted to determine an exact $\lambda(T_b, T_{ub})$.

[39] 6. When primary NRM is partially remagnetized, only a multivectorial Arai plot will give correct paleofield estimates for both primary and secondary remanences. Finding directions for both remanences from their demagnetization trajectories is a prerequisite to separating their Thellier data and obtaining trustworthy paleointensities. This is only possible for SD or nearly SD grains with

minimal overlap between the T_{ub} spectra of the two remanences.

[40] **Acknowledgments.** This research has been supported by the Natural Sciences and Engineering Research Council of Canada through grant A7709 to D.J.D. We thank Andrew Biggin and David Krása for careful and helpful reviews which improved the paper.

References

Aitken, M. J., A. L. Allsop, G. D. Bussell, and M. B. Winter (1988), Determination of the intensity of the Earth's magnetic field during archeological times: Reliability of the Thellier technique, *Rev. Geophys.*, *26*, 3–12.

Biggin, A. J., and H. N. Böhnel (2003), A method to reduce the curvature of Arai plots produced during Thellier paleointensity experiments performed on multidomain grains, *Geophys. J. Int.*, *155*, F13–F19.

Bol'shakov, A. S., and V. V. Shcherbakov (1979), A thermomagnetic criterion for determining the domain structure of ferrimagnetics, *Izv. Russ. Acad. Sci. Phys. Solid Earth, Engl. Transl.*, *15*, 111–117.

Carlut, J., and D. V. Kent (2002), Grain size dependent paleointensity results from very recent mid-oceanic ridge basalts, *J. Geophys. Res.*, *107*(B3), 2049, doi:10.1029/2001JB000439.

Carvallo, C., P. Camps, G. Ruffet, B. Henry, and T. Poidras (2003), Mono Lake or Laschamp geomagnetic event recorded from lava flows in Amsterdam Island (southeastern Indian Ocean), *Geophys. J. Int.*, *154*, 762–782.

Coe, R. S. (1967), Paleointensities of the Earth's magnetic field determined from Tertiary and Quaternary rocks, *J. Geophys. Res.*, *72*, 3247–3262.

Dunlop, D. J. (1983), Viscous magnetization of 0.04–100 μm magnetite, *Geophys. J. R. Astron. Soc.*, *74*, 667–687.

Dunlop, D. J. (2003), Partial thermoremanent magnetization: Louis Néel's legacy in rock magnetism, *J. Appl. Phys.*, *93*, 8236–8240.

Dunlop, D. J., and Ö. Özdemir (1997), *Rock Magnetism: Fundamentals and Frontiers*, 573 pp., Cambridge Univ. Press, New York.

Dunlop, D. J., and Ö. Özdemir (2000), Effect of grain size and domain state on thermal demagnetization tails, *Geophys. Res. Lett.*, *27*, 1311–1314.

Dunlop, D. J., and Ö. Özdemir (2001), Beyond Néel's theories: Thermal demagnetizations of narrow-band partial thermoremanent magnetization, *Phys. Earth Planet. Inter.*, *126*, 43–57.

Dunlop, D. J., and G. F. West (1969), An experimental evaluation of single domain theories, *Rev. Geophys.*, *7*, 709–757.

Dunlop, D. J., Ö. Özdemir, and P. W. Schmidt (1997), Paleomagnetism and paleothermometry of the Sydney Basin: 2. Origin of anomalously high unblocking temperatures, *J. Geophys. Res.*, *102*, 27,285–27,295.

Dunlop, D. J., B. Zhang, and Ö. Özdemir (2005), Linear and nonlinear Thellier paleointensity behavior of natural minerals, *J. Geophys. Res.*, *110*, B01103, doi:10.1029/2004JB003095.

Fabian, K. (2000), Acquisition of thermoremanent magnetization in weak magnetic field, *Geophys. J. Int.*, *142*, 478–486.

Fabian, K. (2001), A theoretical treatment of paleointensity determination experiments on rocks containing pseudo-single or multi domain magnetic particles, *Earth Planet. Sci. Lett.*, *188*, 45–58.

Halgedahl, S. L. (1993), Experiments to investigate the origin of anomalously elevated unblocking temperatures, *J. Geophys. Res.*, *98*, 22,443–22,460.

Kirschvink, J. L. (1980), The least-squares line and plane and the analysis of paleomagnetic data, *Geophys. J. R. Astron. Soc.*, *62*, 699–718.

Krása, D., C. Heunemann, R. Leonhardt, and N. Petersen (2003), Experimental procedure to detect multidomain remanence during Thellier-Thellier experiments, *Phys. Chem. Earth*, *28*, 681–687.

Leonhardt, R., D. Krása, and R. S. Coe (2004), Multidomain behavior during Thellier paleointensity experiments: A phenomenological model, *Phys. Earth Planet. Inter.*, *147*, 127–140.

Levi, S. (1977), The effect of magnetite particle size on paleointensity determinations of the geomagnetic field, *Phys. Earth Planet. Inter.*, *13*, 245–259.

Levi, S. (1979), The additivity of partial thermal remanent magnetization in magnetite, *Geophys. J. R. Astron. Soc.*, *59*, 205–218.

Markov, G. P., V. P. Shcherbakov, A. S. Bol'shakov, and Y. K. Vinogradov (1983), On the temperature dependence of the partial thermoremanent magnetization of multidomain grains, *Izv. Russ. Acad. Sci. Phys. Solid Earth, Engl. Transl.*, *19*, 625–630.

McClelland, E., and N. Sugiura (1987), A kinematic model of TRM acquisition in multidomain magnetite, *Phys. Earth Planet. Inter.*, *46*, 9–23.

McClelland, E., A. R. Muxworthy, and R. M. Thomas (1996), Magnetic properties of the stable fraction of remanence in large multidomain (MD) magnetite grains: Single-domain or MD?, *Geophys. Res. Lett.*, *23*, 2831–2834.

Middleton, M. F., and P. W. Schmidt (1982), Paleothermometry of the Sydney basin, *J. Geophys. Res.*, *87*, 5351–5359.

Muxworthy, A. R. (2000), Cooling behavior of partial thermoremanences induced in multidomain magnetite, *Earth Planet. Sci. Lett.*, *184*, 169–179.

Nagata, T., Y. Arai, and K. Momose (1963), Secular variation of the geomagnetic total force during the last 5000 years, *J. Geophys. Res.*, *68*, 5277–5281.

Ozima, M., and M. Ozima (1965), Origin of thermoremanent magnetization, *J. Geophys. Res.*, *70*, 1363–1369.

Preisach, F. (1935), Über die magnetische Nachwirkung, *Z. Phys.*, *94*, 277–302.

Shashkanov, V. A., and V. V. Metallova (1977), Determination of paleointensity from sedimentary and igneous rocks by the method of alternating-field remagnetization, *Phys. Earth Planet. Inter.*, *13*, 368–372.

Shcherbakov, V. P., and V. V. Shcherbakova (2001), On the suitability of the Thellier method of paleointensity determination on pseudo-single-domain and multidomain grains, *Geophys. J. Int.*, *146*, 20–30.

Shcherbakov, V. P., and V. V. Shcherbakova (2002), The paleomagnetic direction determination: Implications of the domain structure of ferromagnetic grains in rocks, *Izv. Russ. Acad. Sci. Phys. Solid Earth, Engl. Transl.*, *38*, 404–411.

Shcherbakov, V. P., and N. K. Sycheva (1997), Fulfillment of the Thelliers' laws of independence and additivity of partial thermoremanent magnetizations for interacting single-domain grains (numerical experiment), *Izv. Russ. Acad. Sci. Phys. Solid Earth, Engl. Transl.*, *33*, 329–334.

Shcherbakova, V. V., V. P. Shcherbakov, P. W. Schmidt, and M. Prévot (1996), On the effect of low-temperature demagnetization on TRMs and pTRMs, *Geophys. J. Int.*, *127*, 379–386.

Shcherbakova, V., V. P. Shcherbakov, and F. Heider (2000), Properties of partial thermoremanent magnetization in PSD and MD magnetite grains, *J. Geophys. Res.*, *105*, 767–782.

Tauxe, L. (1998) *Paleomagnetic Principles and Practice*, 299 pp., Springer, New York.

Thellier, E. (1938), Sur l'aimantation des terres cuites et ses applications géophysiques, *Ann. Inst. Phys. Globe Univ. Paris Bur.*, *16*, 157–302.

Thellier, E., and O. Thellier (1959), Sur l'intensité du champ magnétique terrestre dans le passé historique et géologique, *Ann. Geophys.*, *15*, 285–378.

Vinogradov, Y. K., and G. P. Markov (1989), On the effect of low temperature heating on the magnetic state of multidomain magnetite, in *Investigations in Rock Magnetism and Paleomagnetism* (in Russian), pp. 31–39, Inst. of the Phys. of the Earth, Moscow.

Worm, H. U., M. Jackson, P. Kelso, and S. K. Banerjee (1988), Thermal demagnetization of partial thermoremanent magnetization, *J. Geophys. Res.*, *93*, 12,196–12,204.

Xu, S., and D. J. Dunlop (2004), Thellier paleointensity theory and experiments for multidomain grains, *J. Geophys. Res.*, *109*, B07103, doi:10.1029/2004JB003024.

Yu, Y., and D. J. Dunlop (2001), Paleointensity determination on the late Precambrian Tudor Gabbro, Ontario, *J. Geophys. Res.*, *106*, 26,331–26,344.

Yu, Y., and D. J. Dunlop (2002), Multivectorial paleointensity determination from the Cordova Gabbro, southern Ontario, *Earth Planet. Sci. Lett.*, *203*, 983–998.

Yu, Y., and D. J. Dunlop (2003), On partial thermoremanent magnetization tail checks in Thellier paleointensity determination, *J. Geophys. Res.*, *108*(B11), 2523, doi:10.1029/2003JB002420.

Yu, Y., and L. Tauxe (2005), Testing the IZZI protocol of geomagnetic field intensity determination, *Geochem. Geophys. Geosyst.*, *6*(5), Q05H17, doi:10.1029/2004GC000840.

Yu, Y., and L. Tauxe (2006), Effect of multi-cycle heat treatment and prehistory dependence on partial thermoremanence (pTRM) and pTRM tails, *Phys. Earth Planet. Inter.*, *157*, 196–207.

Yu, Y., D. J. Dunlop, and Ö. Özdemir (2003), Testing the independence law of partial ARMs: Implications for paleointensity determination, *Earth Planet. Sci. Lett.*, *208*, 27–39.

Yu, Y., L. Tauxe, and A. Genevey (2004), Toward an optimal geomagnetic field intensity determination technique, *Geochem. Geophys. Geosyst.*, *5*(2), Q02H07, doi:10.1029/2003GC000630.

D. J. Dunlop, Geophysics, Department of Physics, University of Toronto, Toronto, ON, Canada M5S 1A7.

Y. Yu, Department of Earth and Environmental Sciences, Korea University, Seoul 136-701, South Korea. (yongjaeyu@naver.com)